
Article:
Thornton, Katie Louise, Findlay, Rachel Christina, Walrad, Pegine Bavonne orcid.org/0000-0002-2302-0720 et al. (1 more author) (2016) Investigating the Swimming of Microbial Pathogens Using Digital Holography. Advances in experimental medicine and biology. pp. 17-32. ISSN 0065-2598

https://doi.org/10.1007/978-3-319-32189-9_3

Chapter 1
Investigating the swimming of microbial pathogens using digital holography

K.L. Thornton, R.C. Findlay, P.B. Walrad & L.G. Wilson

Abstract To understand much of the behaviour of microbial pathogens, it is necessary to image living cells, their interactions with each other and with host cells. Species such as *Escherichia coli* are difficult subjects to image: they are typically microscopic, colourless and transparent. Traditional cell visualisation techniques such as fluorescent tagging or phase-contrast microscopy give excellent information on cell behaviour in two dimensions, but no information about cells moving in three dimensions. We review the use of digital holographic microscopy for three-dimensional imaging at high speeds, and demonstrate its use for capturing the shape and swimming behaviour of three important model pathogens: *E. coli*, *Plasmodium* spp. and *Leishmania* spp.

Key words: Optical microscopy · Holography · Image analysis · Leishmania · Plasmodium

Katie L. Thornton
Department of Physics, University of York, Heslington, York, YO10 5DD, e-mail: klt531@york.ac.uk

Rachel C. Findlay
Centre for Infection & Immunity, Department of Biology and Department of Physics, University of York, Heslington, York, YO10 5DD e-mail: rcf511@york.ac.uk

Pegine B. Walrad
Centre for Infection & Immunity, Department of Biology, University of York, Heslington, York, YO10 5DD e-mail: pegine.walrad@york.ac.uk

Laurence G. Wilson
Department of Physics, University of York, Heslington, York, YO10 5DD, e-mail: laurence.wilson@york.ac.uk

1.1 Introduction

Microbial pathogens are responsible for the majority of annual mortality and morbidity. A high-profile example is malaria, which infects around 200 million people, primarily in the developing world [1]. Pathogens responsible for malaria and other diseases have diverse evolutionary histories found in both the bacterial and eukaryotic domains[1]. For many pathogens, cell motility is an important means of facilitating infection. The ability to move allows extension of territory, search for nutrients and avoidance of host immune response.

Studies of pathogenic cell motility have long been dictated by the experimental tools available. Optical microscopes have been central in this effort, and have undergone extensive refinement. Microscope objective lenses are now highly optimised, and allow the operator to image objects separated by as little as half a wavelength — a limitation set by the fundamental physics of waves and known as the diffraction limit. Advances in contrast generation techniques such as Zernike phase contrast [3] or differential interference contrast [4] have improved image fidelity, and biochemistry has played a role in developing new variant markers and stains to facilitate the visualisation of microscopic subjects under fluorescent illumination. Recently, super-resolution techniques have provided a way to beat the diffraction limit, imaging structures in the 10 nm size range, through the combined advancement of laser illumination with digital image sensors and computing technology.

In fact, digital sensors and high-performance microscopes are nearly ubiquitous in modern microbiology labs. This equipment is often used for routine sample screening and documentation, but provides other opportunities for quantitative measurements. Video tracking of particles or cells [5] gives a single-cell resolution picture of motility, while scattering-based methods can assay motility in a larger population [6, 7]. Another example is digital inline holographic microscopy (DIHM). Although this method was first described some twenty years ago [8], computing power has recently developed to the stage that DIHM can be routinely implemented in desktop machines. There are two distinct implementations of this method: a quantitative phase contrast method to assess the axial thickness of microscopic subjects [9, 10, 11]; and a method for three-dimensional localisation and imaging of objects [12, 13, 14, 15]. This paper concentrates on the latter, and its application to microbial pathogens.

Different forms of cellular motility are observed among microbial cells, with the exact mode dictated to some extent by the cell's environment. Within one species, several different methods for movement may exist, triggered by distinct environmental context. *E. coli*, implicated in over half of urinary tract infections in a recent study based in Canada [16], demonstrates a strong connection between motility and ability to infect patients. *E. coli* cells are capable

[1] Although, intriguingly, not yet among the archaea [2].

of swimming freely in a liquid, propelled by a helical bundle of thin flagellar filaments. When present on surfaces in sufficient numbers, the cells grow longer and produce more flagella, becoming hyper-flagellated swarmer cells that swim at increased speeds within surface fluid films. These modes of motion — certainly swimming, and possibly swarming too — can be modulated by a chemical-sensing response (chemotaxis). This allows cells to navigate to more favourable environments. A variety of motility strategies convey competitive advantages. Studies have revealed that efficient swimming behaviours and chemotactic responses are highly beneficial in the early colonisation of the urinary tract, bladder and kidney, and may provide an increase in fitness essential for competition with other pathogens [17, 17]. Beyond swimming and swarming, bacterial motions include 'twitching' in *Pseudomonas aeruginosa* and 'gliding' in *Flavobacterium* and *Mycoplasma* [18, 19].

Eukaryotic pathogens also display a diverse range of motilities. Some of the most rapid swimming motion exhibited by eukaryotes is due to the action of eukaryotic flagella, or motile cilia[2]. These whip-like organelles are widely conserved across the eukaryotes, and are found in plants, animals, fungi and protozoa. Eukaryotic flagella are distinct from their bacterial and archaeal counterparts in terms of their more sophisticated internal machinery (the bacterial and archaeal appendages are simply rigid propellers), and consequently, their size. The underlying structure of eukaryotic flagella, known as the axoneme, is a 200 nm-diameter cylinder of microtubule doublets bridged by dynein molecules. These dynein 'molecular motors' cause the doublets to shift longitudinally with respect to each other, causing bending waves that run along the whole structure. This outer cylinder sometimes surrounds microtubule singlets, which can occur individually, in pairs or in triplets. The exact role of these additional microtubules remains obscure, although they have been implicated in beat regulation and may help to define an anisotropic bending rigidity. Other internal machinery along the axoneme is responsible for transporting protein cargo to the flagellum's proximal and distal ends, although this is not present in all species.

The molecular motors that allow flagellar motion act in concert to deform the flagellum, creating a beating stroke that pumps external fluid. Observing flagella in action, and understanding the physics and biology of their operating mechanism is a key challenge in modern biophysics. The complex life cycles of some of the most medically-relevant eukaryotic parasites requires cells to move in hostile environments. This motion is enabled in several key cases by the adaptation and action of eukaryotic flagella. Parasites such as *Plasmodium* spp. and *Leishmania* spp. (responsible for malaria and leishmaniasis, respectively) encounter a range of physical and chemical challenges in their journeys through insect vectors and vertebrate hosts. In doing so, the cells radically remodel their physiology to adapt to external conditions. A striking example is the sexually reproductive stage of *Plasmodium*'s life

[2] Eukaryotic flagella and motile cilia are structurally very similar; their names appear to be used somewhat interchangeably within the motility literature.

cycle. Here, the male gametocyte of the intracellular parasite synthesizes eukaryotic flagella when taken up into the insect vector's midgut. These flagellated *Plasmodium* parasites, also known as microgametes, must leave the red blood cell in which they were synthesised and convey nuclear material through a dense blood meal to find their female counterparts. This is the only motile form of the parasite's life cycle, and its motility is known to be critical to the parasite's survival [20]. To study the motility of *Plasmodium* in this sexual reproduction stage, we have used the rodent-infecting species *Plasmodium berghei* [21].

Leishmania are protozoan parasites able to infect human leukocytes and cause a range of clinical symptoms, from minor skin lesions to fatal visceral disease [22]. Although our current understanding of host-pathogen interaction is incomplete, the life cycle of *Leishmania* has been well characterised. There are two basic life cycle forms of *Leishmania*: the amastigote form is an obligate intracellular, non-motile form which multiplies by binary fission within mammalian host cells, the promastigote form is a flagellated, extracellular form which infects the sandfly vector [23]. In the sandfly, the amastigotes transform into weakly motile procyclic promastigotes which have a flagellum the same size as the cell body localised at their anterior end of the cell. The assembly of a flagellum in the promastigotes allows for the motility and attachment in the sandfly's gut and is critical for the parasite's transmission through the vector [24] and into the mammalian hosts. These procyclic parasites replicate and migrate towards the anterior midgut and foregut of the fly. Most individuals transform into non-replicating metacyclic promastigotes, which have increased motility in culture possibly due to an elongated flagellum twice the length of the cell body, at the anterior end [25]. A gel secreted by the promastigotes (PSG) creates a plug forcing the sand fly's stomodeal valve to open and extend into the pharynx. The fly then regurgitates and expels the PSG along with metacyclic promastigotes into the host it has bitten [26].

The molecular aspects of this infection process are relatively well known and several host cell receptors that recognise the parasite's surface molecules have been identified [22, 27]. However, much of the parasite cell biology is poorly understood, specifically the involvement of motility in the processes of parasite attachment and engulfment by host macrophages [28]. A recent study highlighted the importance of the role of promastigote polarity and motility during parasite entry to host cells [23]. Using high spatiotemporal resolution microscopy to image an infection assay it was shown the motile promastigotes enter the macrophages in a polarized manner through their flagellar tip. The persistent intracellular flagellar activity is thought to lead to reorientation of the parasite flagellum towards the host cell periphery resulting in oscillatory parasite movement. The *Leishmania* infection process is assumed to rely on the phagocytic capacity of the host cell [23]. Thus, understanding how morphology and motility of the promastigote parasites

affect macrophage colonisation may provide important insights into *Leishmania* spp. infection.

Three key species described above — *E. coli*, *P. berghei* and *L. mexicana* — are shown in Fig. 1.1, alongside some relevant motility characteristics. We have used DIHM to study all three; we present some results below, with a brief discussion of the physical principles of holography and practical experimental considerations.

Organism	Normalised Holographic Image	Physical Features
Escherichia coli 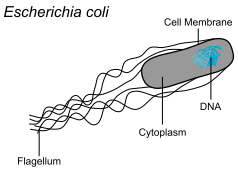	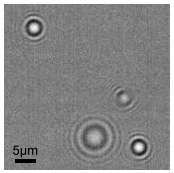	• Body size ~ 2 x 1 µm • Flagellar filaments measure ~ 6-10 µm in length, ~ 20 nm in diameter • Cells peritrichously flagellated, 6-10 flagella per cell • Flagellar rotation rate ~ 100 Hz • Swimming speed ~ 20 µm/s
Plasmodium berghei 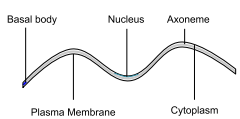	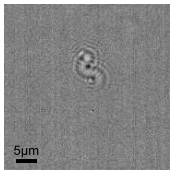	• Free swimming eukaryotic flagellum • Length ~ 8-12 µm, diameter ~ 250 nm • Nuclear material inside flagellum • Flagellar beat frequency ~ 10 Hz • Swimming speed ~ 5 µm/s
Leishmania mexicana 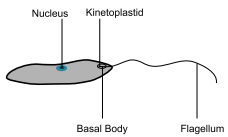	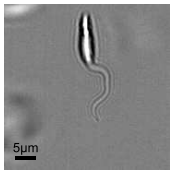	• Body size ~ 10 x 2 µm (procyclic promastigote) • Eukaryotic flagellum ~ 15 µm in length, 250 nm diameter • One flagellum per cell • Flagellar beat frequency ~ 30 Hz • Swimming speed ~ 35 µm/s

Fig. 1.1 Table showing three pathogens studied using DIHM. *Top row: E. coli* bacteria, showing an example holographic image and characteristic physical parameters dimensions. *Middle row: P. berghei* microgamete. These cells are essentially an isolated eukaryotic flagellum with nuclear material distributed along the length of the axoneme, inside the cell membrane. *Bottom row: Leishmania mexicana* procyclic promastigote. The relatively large cell body can be clearly seen in the raw data (centre panel).

1.1.1 Optics Background

The study of optics is one of the oldest branches of physics, certainly dating back to antiquity [3]. The description of light as oscillations in an electromagnetic field is 19^{th} century physics, and our understanding of how light is detected, both by our eyes and by electronic sensors, is now well established. Oscillations in an electric field are conveniently described as sinusoidal waves, with well-defined amplitude and phase (position in the wave cycle). Almost all light-recording material — the retina, photographic film, digital imaging sensors — are sensitive to the *intensity* of incident light (given by the amplitude squared), but not the phase. As a result, phase information is lost in the process of recording an optical field by conventional means. This is not generally a serious issue; human perception is used to analysing data from the intensity of optical fields, and so photographs and digital images are perfectly intelligible.

There are ways of capturing the phase information, however, and holography is one example. Holography was originally developed by Dennis Gabor [29] as a method of correcting aberrations in an electron microscope (in which the electrons can be thought of as waves), but has subsequently been applied to optical and acoustic imaging as well [30]. The word 'holography' comes from the Greek *'holos'*, meaning whole. This is appropriate because the phase and amplitude information that a hologram contains is sufficient to reconstruct the optical field at any other point along its propagation direction. There are many different methods for achieving reconstruction, even in the field of microscopy, but we will focus on DIHM, as it is one of the simplest and most robust microscopic holographic imaging methods.

Interference between two waves is the central concept in holography: a light wave scattered by an object of interest (the 'object wave') is superimposed on to a wave with a known phase (the 'reference wave'). This reference wave is often a plane wave, in which the phase is constant across any plane perpendicular to the direction of propagation. When the electric fields of the object and reference waves combine, they produce an interference pattern of light and dark fringes, corresponding to constructive or destructive interference. This interference pattern reveals the phase of the object wave, as compared the the quasi-constant reference, and encodes phase differences within the recorded amplitude. Examples of holographic images can be seen in the central column of Fig. 1.1, in which the cells' rough outlines can be discerned, surrounded by light and dark fringes. These images were obtained using a DIHM setup with LED illumination, as shown in Fig. 1.2**a**, which we describe in more detail in the next section.

1.1.2 Optical setup

Figure 1.2 shows two alternative geometries for an inline holographic microscope. Both of the geometries are based on a standard commercial inverted microscope; the only deviation from standard bright field microscopy is in the illumination assembly. Figure 1.2**a** shows a setup in which an LED is used as a light source, and the nearly-closed condenser aperture is used to create a point-like source in the back focal plane of the condenser lens. The lens turns the point-source emission into plane waves at the sample, as indicated. The alternative setup in Fig. 1.2**b** uses a laser for illumination, coupled to a single-mode optical fibre. The fibre is held at a distance of 2–5 cm above the sample, meaning that the optical field is well approximated as a plane wave when it is incident on the sample. Note that the condenser lens is unnecessary in this second setup, as laser sources can have high intensity, and don't require collimation, unlike the LED source. When light passes through either system, some of it is scattered by objects in the sample. This scattered light (the object wave) interferes with the remaining unscattered light (the reference wave) at the image plane. The fact that the object and reference wave both take substantially the same path through the imaging system is the reason why these geometries are described as 'inline' holographic microscopes.

The two configurations shown in Fig. 1.2 take advantage of the different levels of optical coherence offered by each source. Optical coherence is a nuanced topic beyond the scope of this article [31], but manifests here as the deviation that the object wave can take from the reference while still producing interference fringes. An LED source has low coherence, so the object and reference wave must be nearly colinear in order to produce fringes. In practice, this means that only a small thickness of the sample volume can be imaged at one time, as indicated in the red highlighted regions in the lower panels of Fig. 1.2 (*L. mexicana* cells drawn to scale). A laser is highly coherent and so can be used to image much thicker sample volumes, at both high and low magnification. At first sight, it would seem that a laser is therefore preferable as a source for producing holographic images, but this isn't always the case. Use of a laser increases the size of the 'sensitive volume' in a DIHM setup, but this includes unwanted contributions from dust particles that cross the optical path during experiments, irregularities on the surface of the sample chamber and other sources that can produce a confounding signal. For the study of small, very weakly scattering subjects, the smaller volume accessed by an LED is more selective and less susceptible to noise from other parts of the experiment.

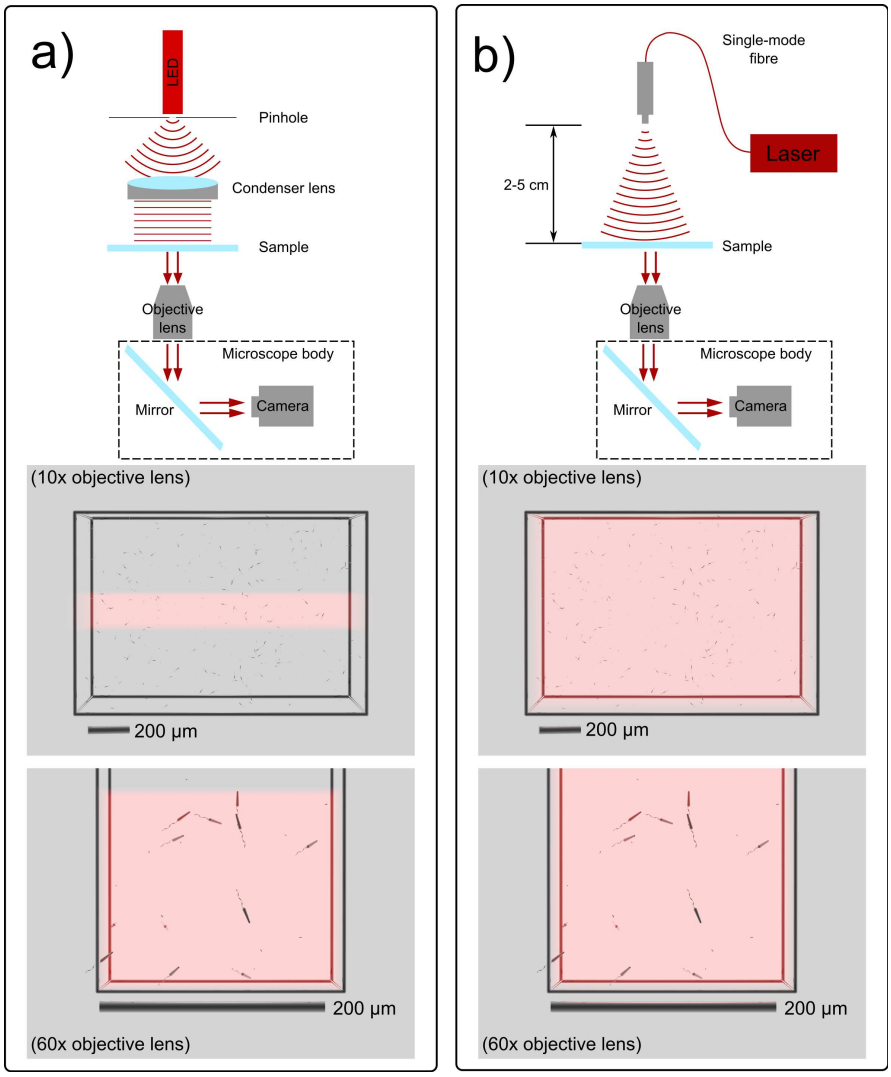

Fig. 1.2 Two layouts for digital inline holographic microscopy (DIHM). At the bottom of each panel are two 'cartoon' image of the sample, highlighting the volume from which data is recorded, using typical 10× and 60× objective lenses. These lower four panels contain 'cartoon' cells, drawn to scale, to represent *Leishmania mexicana* and *E. coli*. The latter are barely visible in each case, due to their small size. The system in panel **a** uses an LED and a pinhole (nearly-closed condenser aperture) for quasi-coherent illumination. Panel **b** uses a diode laser coupled to a single mode fibre, which eliminates the need for a pinhole.

1.1.3 Data processing

Raw DIHM images are 2-dimensional and look similar to out-of-focus bright field microscope images (see Fig. 1.1). These images contain information about the three-dimensional positions and shapes of the cells in the sample chamber. There are several computational processing schemes for extracting three-dimensional information from holographic images [32, 33], but we have found the Rayleigh-Sommerfeld back-propagation method [34] to be the most convenient. This method treats the holographic image as a plane in three-dimensional space. It takes every pixel in the raw image as a source of light waves, each with the same phase, and an amplitude set by the pixel value (a light pixel is a strong source, a dark pixel is a weak one). By summing the contributions from all sources at a particular point some distance from the raw image, it is possible to reconstruct the original optical field at that position. Repeating this summation at several points across a plane parallel to the holographic image, we 'numerically refocus' the raw image at an arbitrary distance within the sample.

In practice, a stack of images is typically produced using this method, which replicates manually scanning the microscope's focal plane through a sample, taking images at different depths into the sample. Weakly-scattering objects appear to have bright or dark centres, depending upon which side of the focal plane they lie on. An object's appearance changes (from light to dark or vice versa) when it passes through the focal plane [35, 36]. Regions where this light-dark transition occurs in a short distance in the axial (z) direction are therefore associated with scattering regions and are used to localise objects in the three-dimensional volume. Each small volume of the object hit by the laser light will scatter some light, and the total scattered field can then be measured as the sum of the individual contributions. This approach is an approximation of the light scattering physics known as the Rayleigh-Gans-Debye (RGD) approximation. RGD scattering is a viable approximation if the scatterer's refractive index relative to the suspending medium ($m = \frac{n_s}{n_m}$) and characteristic dimension, d, adheres to the following conditions:

$$|m-1| \ll 1, \qquad \text{and} \qquad kd|m-1| \ll 1, \tag{1.1}$$

where the wavenumber $k = 2\pi n_m/\lambda$, and λ is the illumination wavelength. Under this assumption each small portion of the subject behaves as an independent scattering centre, scattering light as if isolated from the rest of the sample. This independence means that each notional scattering centre appears in the refocused image stack as a localised region in which there is a dark-to-light transition as the image is numerically refocused. These dark-to light transitions are isolated in an image stack using a three-dimensional image processing filter based on the two-dimensional Sobel-Feldman operator [35]. The use of this operator transforms a stack of numerically refocused

images into one in which axial intensity gradients are picked out as bright objects on a dark background. The objects are simple to isolate by performing a thresholding operation on the image stack. Multiple scattering centres within the same extended object can be associated with each other, or single scattering centres tracked over time, as seen in the next section.

1.1.4 Example results

The holographic recording and reconstruction process described in the previous section results in data that can be analysed at a range of different length scales. Previous studies have broadly taken one of two approaches: examine the shape of single cells at high resolution, or establish a 'centroid' position within the cell and track this over time. We will give examples of both in the following sections, but note that the intermediate length scale (larger than a cell, but smaller than a sample chamber) could be a fruitful area for future investigation.

1.1.4.1 Long range tracking

The description in previous sections, and references therein, concern how an object can be localised within a reconstructed optical field. At low magnification, single cells appear point-like. At low cell concentrations and high enough video frame rates, individual points can be tracked across multiple frames, to provide information on the swimming patterns of cells [37]. This type of information is shown in Fig. 1.3**a**–**d**. The data show the track of a single *E. coli* cell as it swims in a sample chamber filled with motility buffer. The cell covers a distance of around 300 μm in a period of 65 seconds, and displays the characteristic 'run and tumble' behaviour of a peritrichously flagellated cell first observed by Berg and Brown [38]. This can be seen as relatively straight trajectories, interspersed with angular turns.

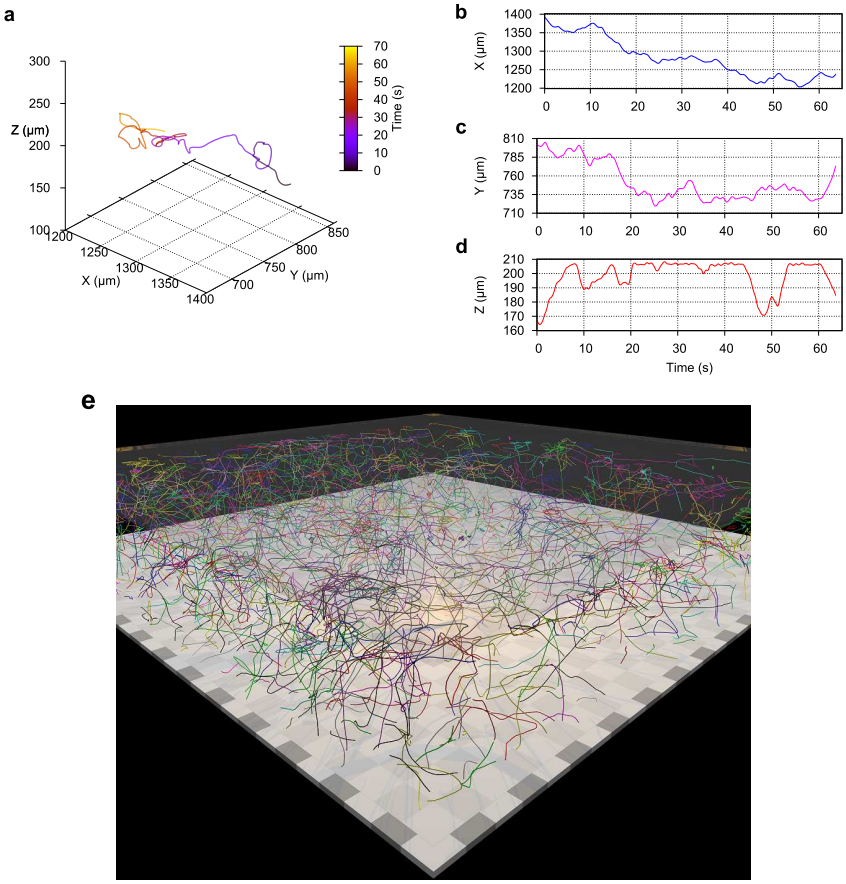

Fig. 1.3 **a** Reconstructed track of a single swimming *E. coli* bacterium , over a period of around 65 seconds (time indicated by the colour of the track). **b**–**d** Single-axis data from the track shown in panel **a**. The height of the sample chamber was around 210 μm, hence the large amount of data close to that position in panel **d**; the cell was hydrodynamically/sterically trapped at this location for some time (see text). **e** Computer rendering of bacterial tracks from over 1000 cells, captured over a period of 80 seconds. The squares on the floor of the rendering represent a distance of 50 μm.

Figure 1.3**a** shows an isometric projection of the three-dimensional track, while Figs. 1.3**b**–**d** show the cell motion in three orthogonal directions, X, Y and Z. The Z (axial) direction is of particular interest, as the cell can be seen colliding with the chamber wall located at $Z \approx 210$ μm. It has been known for some time that swimming cells such as *E. coli* and *Caulobacter crescentus* are influenced by the presence of a wall [39], and often become confined to surfaces as a result of hydrodynamic [40] or steric (geometrical) constraints. Moreover, recent results using holographic microscopy [41] have demonstrated that aside of physical constraints, the cell biophysics is also

affected by the presence of a nearby wall, which suppresses tumbling events in *E. coli*. This result would not have been accessible without the rapid three-dimensional tracking afforded by DIHM.

At relatively low cell concentrations, many cells can be tracked simultaneously. Figure 1.3**e** shows over 1000 tracks, all from an 80 second video acquired at 50 frames per second. The video resolution was 1024×1024 pixels, and using our 10× magnification objective lens, this corresponds to a field of view of 1440 × 1440 μm. The computer rendering in the figure is drawn to scale; the grey/white squares on the ground represent 50 μm, showing the extent of the bacterial motion over this time. The tracks are not all the same length, as some cells swim faster than others, and cells may swim into and out of the field of view (horizontally) during recording. Nevertheless, data on the position of each bacterium as a function of time makes it easy to obtain parameters such as swimming speed, both on a single-cell level and across a population. This information offers insight into how cells spread into new territory, and interact with each other and their environment.

1.1.4.2 High resolution shape studies

At higher magnification, the shape of individual cells can be examined in three dimensions. Eukaryotic flagella are an ideal subject for this type of analysis, as they are weakly scattering, ensuring that the RGD scattering limit is valid. We have used DIHM on *P. berghei* microgametes [42] and cells of *L. mexicana*, to examine the shape and dynamics of the flagellum. Example data from both species can be seen in Fig. 1.4. Figure 1.4**a** shows the DIHM reconstruction procedure, from raw data (on the left) through to the fitted contour that represents the shape of the microgamete (on the right hand side). Assuming that the microtubules are bound together at one end (the 'no basal sliding' approximation), the relative displacement of microtubules within the microgamete can be extracted from the flagellar shape, as seen in Fig. 1.4**b**. The colour map shows the sliding of microtubule doublets in the axoneme relative to the gamete centre line, from the relatively passive 'tail' end of the microgamete (position $s = 0$ μm on the horizontal axis) to the more active head end ($s = 9$ μm). The vertical axis maps position around the circumference of the microgamete, with an angle as indicated in the left-hand panel of Fig. 1.4**b**. A bright yellow band extends from bottom left to top right of the sliding map; this helical wave of microtubule sliding gives rise to the helical waveform seen in the rendering on the left.

DIHM on the *L. mexicana* cells is more challenging due the presence of a cell body that scatters light more strongly than the flagellum. Some example data are shown in Fig. 1.4**c**, where the raw data are on the left, and the reconstructed shape can be seen on the right. The lower object in the reconstruction is the raw data; note the rather noisy data surrounding the position of the cell body. Fortunately, the cell body shape of any one indi-

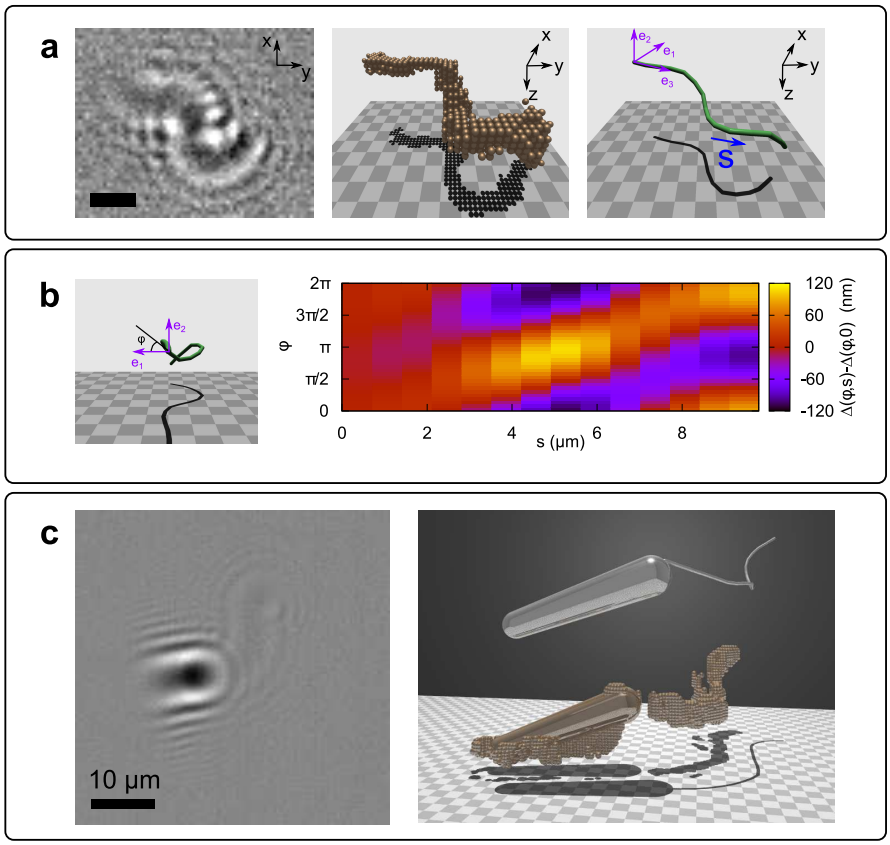

Fig. 1.4 **a** Three stages in reconstructing the shape of a *P. berghei* microgamete. The left-hand image is raw holographic data, scale bar 3 μm; the central panel shows the reconstructed voxels (volume pixels) that indicate the volume in which the microgamete is most likely located; the right-hand panel shows the fitted configuration of the microgamete, subject to known constraints of length and width. **b** Geometric analysis of one particular frame of data from a *P. berghei* microgamete. The left-hand panel shows the reconstruction of the raw holographic data, and the right-hand panel shows the best estimate of inter-tubule sliding that has to occur in order to achieve this waveform geometry. **c** Raw holographic data from a procyclic cell of *L. mexicana*. The cell body scatters light much more strongly than the flagellum, and is surrounded by higher-contrast fringes. The panel on the right shows the best estimate of the cell body position, and the shape of the flagellum obtained a modified version of the routine used to fit the malaria microgametes. The squares on the floor of the reconstructed image represent 1 μm. *[Panels a & b reproduced from Ref. [42]].*

vidual is constant on the time scale necessary for observing flagellar beating, simplifying analysis somewhat. The ability to study swimming behaviour on a single-cell level in these parasitic species offers new insight into the way that cells move during a critical phase of their life cycles [43]. High-quality

data on the motion of these cells allows us to test existing models of how eukaryotic flagella work [44, 45], which in turn could lead to new pathways for treatment.

1.1.5 Discussion and outlook

We have outlined a few ways in which DIHM can be used to study motile microbial pathogens. The advantages of DIHM are three-fold: (i) the low cost of the apparatus required, (ii) the availability of free software algorithms for post-processing, and (iii) the unique information offered by high-speed, three-dimensional imaging.

The first of these advantages is clear from the optical layout schemes shown in Fig. 1.2. An existing optical microscope may be altered in order to perform DIHM, simply by changing the light condenser array to introduce an alternative illumination source. Any CMOS or CCD camera can be used for imaging, as shown in recent studies that have used cellphone cameras in to perform DIHM in a field-ready instrument [46]. The second advantage is one that is becoming increasingly important in the adoption of image processing standards. Programmes such as ImageJ [47] can be freely downloaded, and custom-written add-ons that provide unique functionality find a broader user base if the source code is made available. The last advantage is probably the most compelling, however. Other competing methods for three-dimensional imaging, such as rapid scanning of the microscope focal plane [48] are technically demanding and only accessible by dedicated experimental apparatus. Laser scanning confocal microscopy is another approach for three-dimensional imaging of microscopic subjects; this scheme allows high- or super-resolution imaging, but typically requires that the subject is fluorescently labelled. Moreover, confocal schemes require the sample to be mechanically translated between axial sections, restricting the speed at which three-dimensional information can be acquired. In the case of multiple freely-swimming cells, DIHM has the distinct advantage because of its high data acquisition rate; this is limited only by the frame rate of the camera used for imaging, and modern cameras with frame rates in excess of 1 kHz at megapixel resolution can be obtained for small fraction of the cost of a confocal scanning system.

DIHM is certainly not without shortcomings, however. The use of lasers invokes the usual safety concerns, especially where optical instruments are involved: even at relatively low beam powers, a microscope can concentrate laser light to levels that are hazardous to the eyes if appropriate safety interlocks are not in place. The resolution of digital holographic microscopy is similar to that of standard bright field microscopy [36], although typically with slightly poorer resolution in the axial direction, and improvements in the resolution are bound by the classical diffraction limit.

Looking towards the future, the biggest single step would be coupling DIHM and fluorescence methods. This would take advantage of increasingly fine biochemical and genetic control over microbiological subjects, allowing experimentalists to label and track structures in three dimensions, and potentially at high speeds. Holography performed with the light emitted by fluorescent subjects has been demonstrated on test samples [49], but will require a significant investment of research effort before it is suitable for use with weakly-fluorescent biological samples, due to serious inefficiencies in the light-gathering optics. Nevertheless, the idea that fluorescently labelled cellular components could be tracked in three dimensions is a compelling one, and would surely enable new insights into the structure and function of microbial pathogens.

References

1. World Health Organization. *World malaria report 2014*. WHO Press, 2014.
2. R. Cavicchioli, P.M.G. Curmi, N. Saunders, and T. Thomas. Pathogenic archaea: do they exist? *Bioessays*, 25(11):1119–1128, 2003.
3. M. Born and E. Wolf. *Principles of Optics, 7th Ed.* Cambridge University Press, 2005.
4. R.D. Allen. New observations on cell architecture and dynamics by video-enhanced contrast optical microscopy. *Ann. Rev. Biophys. Biophys. Chem*, 14:265–290, 1985.
5. J C Crocker and D G Grier. Methods of digital video microscopy for colloidal studies. *J. Colloid Interface Sci.*, 179:298–310, 1996.
6. L. G. Wilson, V. A. Martinez, J. Schwarz-Linek, J. Tailleur, G. Bryant, P. N. Pusey, and W. C. K. Poon. Differential dynamic microscopy of bacterial motility. *Phys. Rev. Lett.*, 106(1):018101, Jan 2011.
7. R. Colin, R. Zhang, and L.G. Wilson. Fast, high-throughput measurement of collective behaviour in a bacterial population. *J. R. Soc. Interface*, 11:20140486, 2014.
8. U. Schnars and W. Jüptner. Direct recording of holograms by a ccd target and numerical reconstruction. *Appl. Opt.*, 33:179–181, 1994.
9. E. Cuche, F. Bevilacqua, and C. Depeursinge. Digital holography for quantitative phase-contrast imaging. *Opt. Lett.*, 24:291–293, 1999.
10. Y.K. Park, W. Choi, Z. Yaqoob, R. Dasari, K. Badizadegan, and M.S. Feld. Speckle-field digital holographic microscopy. *Opt. Express*, 17(15):12285–12292, 2009.
11. C. Edwards, R. Zhoui, S.-H. Hwang, S.J. McKeown, K. Wang, B. Bhaduri, R. Ganti, P.J. Yunker, A.G. Yodh, J.A. Rogers, L.L. Goddard, and G. Popescu. Diffraction phase microscopy: monitoring nanoscale dynamics in materials science. *Appl. Optics*, 53(27):G33–G43, 2014.
12. W. Xu, M. H. Jericho, I. A. Meinertzhagen, and H. J. Kreuzer. Digital in-line holography for biological applications. *Proc. Natl. Acad. Sci.*, 98(20):11301–11305, 2001.
13. J. Fung, K. E. Martin, R. W. Perry, D. M. Katz, R. McGorty, and V. N. Manoharan. Measuring translational, rotational, and vibrational dynamics in colloids with digital holographic microscopy. *Opt. Express*, 19(9):8051–8065, 2011.
14. T.W. Su, L. Xue, and A. Ozcan. High-throughput lensfree 3d tracking of human sperms reveals rare statistics of helical trajectories. *Proc. Natl. Acad. Sci.*, 109:16018–16022, 2012.
15. F. Merola, L. Miccio, P. Memmolo, G. Di Caprio, A. Galli, R. Puglisi, D. Balduzzi, G. Coppola, P. Netti, and P. Ferraro. Digital holography as a method for 3d imaging and estimating the biovolume of motile cells. *Lab Chip*, 13:4512–4516, 2013.

16. B. Foxman. The epidemiology of urinary tract infection. *Nat. Rev. Urol.*, 7:653–660, 2010.
17. K.J. Wright, P.C. Seed, and S.J. Hultgren. Uropathogenic *escherichia coli* flagella aid in efficient urinary tract colonization. *Infect. Immun.*, 73(11):7657–7668, 2005.
18. A. Shrivastava, P.P. Lele, and H.C. Berg. A rotary motor drives *flavobacterium* gliding. *Curr. Biol.*, 25:338–341, 2015.
19. D. Nakane and M. Miyata. *Mycoplasma mobile* cells elongated by detergent and their pivoting movements in gliding. *J. Bacteriol.*, 194(1):122–130, 2012.
20. A.M. Talman, J.H. Prieto, S. Marques, C. Ubaida-Mohien, M. Lawniczak, M.N. Wass, T. Xu, R. Frank, A. Ecker, R.S. Stanway, S. Krishna, M.E.J. Sternberg, G.K. Christophides, D.R. Graham, R.R. Dinglasan, J.R. Yates III, and R.E. Sinden. Proteomic analysis of the *plasmodium* male gamete reveals the key role for glycolysis in flagellar motility. *Malaria J.*, 13:315, 2014.
21. M.N. Wass, R. Stanway, A.M. Blagborough, K. Lal, J.H. Prieto, D. Raine, M.J.E. Sternberg, A.M. Talman, F. Tomley, J. Yates III, and R.E. Sinden. Proteomic analysis of *plasmodium* in the mosquito: progress and pitfalls. *Parasitology*, 139:1131–1145, 2012.
22. P. Kaye and P. Scott. Leishmaniasis: complexity at the host-pathogen interface. *Nat. Rev. Micriobiol.*, 9:604–615, 2011.
23. C.-L. forestier, C. Machu, C. Loussert, P. Pescher, and G.. F. Späth. Imaging host cell-leishmania interaction dynamics implicates parasite motility, lysosome recruitment, and host cell wounding in the infection process. *Cell Host & Microbe*, 9(4):319–330, 2011.
24. P.A. Bates and P.A. Rogers. New insights into the developmental biology and transmission mechanisms of *leishmania*. *Curr. Mol. Med.*, 4:601–609, 2004.
25. D. M. Mosser and A. Brittingham. *Leishmania*, macrophages and complement: a tale of subversion and exploitation. *Parasitology*, 115:S9–S23, 1997.
26. M. Rogers, P. Kropf, B.-S. Choi, R. Dillon, M. Podinovskaia, P. Bates, and I. Müller. Proteophosophoglycans regurgitated by *leishmania*-infected sand flies target the l-arginine metabolism of host macrophages to promote parasite survival. *Microbes Infect.*, 5:e1000555, 2009.
27. M.E. Rogers, K. Corware, I. Müller, and P.A. Bates. *Leishmania infantum* proteophosphoglycans regurgitated by the bite of its natural sand fly vector, *lutzomyia longipalpis*, promote parasite establishment in mouse skin and skin-distant tissues. *Microbes Infect.*, 12:875–879, 2010.
28. M.E. Rogers. The role of *leishmania* proteophosphoglycans in sand fly transmission and infection of the mammalian host. *Front. Microbiol.*, 3:223, 2012.
29. D. Gabor. A new microscopic principle. *Nature*, 161(161):18275–18282, May 1948.
30. J. W. Goodman. *Introduction to Fourier Optics, 3rd Ed.* Roberts & Company, 2005.
31. L. Mandel and E. Wolf. *Optical Coherence and Quantum Optics*. Cambridge University Press, 1995.
32. S.H. Lee, Y. Roichman, G.-R. Yi, S.-H. Kim, S.-M. Yang, A. van Blaaderen, P. van Oostrum, and D. G. Grier. Characterizing and tracking single colloidal particles with video holographic microscopy. *Opt. Express*, 15(26):18275–18282, 2007.
33. M.K. Kim. Principles and techniques of digital holographic microscopy. *SPIE Rev.*, 1:018005, 2010.
34. S.-H. Lee and D. G. Grier. Holographic microscopy of holographically trapped three-dimensional structures. *Opt. Express*, 15(4):1505–1512, 2007.
35. Laurence Wilson and Rongjing Zhang. 3d localization of weak scatterers in digital holographic microscopy using rayleigh-sommerfeld back-propagation. *Opt. Express*, 20(15):16735–16744, 2012.
36. C.B. Giuliano, R. Zhang, and L.G. Wilson. Digital inline holographic microscopy (dihm) of weakly-scattering subjects. *J. Vis. Exp.*, 84:e50488, 2014.

37. J.F. Jikeli, L. Alvarez, B.M. Friedrich, L.G. Wilson, R. Pascal, R. Colin, M. Pichlo, A. Rennhack, C. Brenker, and U.B. Kaupp. Sperm navigation along helical paths in 3d chemoattractant landscapes. *Nat. Commun.*, 6:7985, 2015.
38. H.C. Berg and D.A. Brown. Chemotaxis in *escherichia coli* analysed by three-dimensional tracking. *Nature*, 239:500, 1972.
39. G. Li and J.X. Tang. Accumulation of microswimmers near a surface mediated by collision and rotational brownian motion. *Phys. Rev. Lett.*, 103:078101, 2009.
40. E. Lauga, W.R. DiLuzio, G.M. whitesides, and H.A. Stone. Swimming in circles: Motion of bacteria near solid boundaries. *Biophys. J.*, 90:400–412, 2006.
41. M. Molaei, M. Barry, R. Stocker, and J. Sheng. Failed escape: Solid surfaces prevent tumbling of *escherichia coli*. *Phys. Rev. Lett.*, 113:068103, 2014.
42. L.G. Wilson, L.M. Carter, and S. E. Reece. High-speed holographic microscopy of malaria parasites reveals ambidextrous flagellar waveforms. *Proc. Natl. Acad. Sci. USA*, 110(47):18769–18774, 2013.
43. K.L. Hill. Biology and mechanism of trypanosome cell motility. *Eukaryot. Cell*, 2(2):200–208, 2003.
44. I.H. Riedel-Kruse, A. Hilfinger, J. Howard, and F. Jülicher. How molecular motors shape the flagellar beat. *HFSP J.*, 1(3):192–208, 2007.
45. C.B. Lindemann. Experimental evidence for the geometric clutch hypothesis. *Curr. Top. Dev. Biol.*, 95:1–31, 2011.
46. O. Mudanyali, D. Tseng, C. Oh, S.O. Isikman, I. Sencan, W. Bishara, C. Oztoprak, S. Seo, B. Khademhosseini, and A. Ozcan. Compact, light-weight and cost-effective microscope based on lensless incoherent holography for telemedicine applications. *Lab Chip*, 10:1417–1428, 2010.
47. C.A. Schneider, W.S. Rasband, and K.W. Eliceiri. Nih image to imagej: 25 years of image analysis. *Nat. Methods*, 9(7):671–675, 2012.
48. G. Corkidi, B. Taboada, C.D. Wood, A. Guerrero, and A. Darszon. Tracking sperm in three-dimensions. *Biochem. Biophys. Res. Comm.*, 373:125–129, 2008.
49. J. Rosen and G. Brooker. Fluorescence incoherent color holography. *Opt. Exp.*, 15:2244–2250, 2007.